Characterization of sodium and potassium adsorption on a faceted Al(111) surface using He-atom scattering

1999 J. Phys.: Condens. Matter 11 5735

(http://iopscience.iop.org/0953-8984/11/30/306)

J. Phys.: Condens. Matter **11** (1999) 5735–5756. Printed in the UK PII: S0953-8984(99)00194-0

Characterization of sodium and potassium adsorption on a faceted Al(111) surface using He-atom scattering

S E Finberg†, J V Lakin†, G Vidali‡ and R D Diehl†

† Physics Department, Penn State University, University Park, PA 16802, USA
‡ Physics Department, Syracuse University, Syracuse, NY 13244-1130, USA

Received 16 December 1998, in final form 28 April 1999

Abstract. He-atom scattering was used to characterize the adsorption properties of Na and K on a faceted Al(111) surface, to gain information about the differences in the growth of alkali metals at different temperatures, and to study the interaction between the He atoms and the surfaces. At 100 K, both Na and K were observed to grow in a layer-by-layer mode on top of the surface, whereas at 300 K, the alkalis intermix with the substrate and do not grow in a layer-by-layer mode. For adsorption at 300 K, the He-atom scattering from facets indicated that the primary step direction on the surface changes from being parallel to $[\bar{1}10]$ to being parallel to $[\bar{1}2\bar{1}]$. The He-atom scattering potentials of the alkali overlayers were in general quite smooth (evidenced by a small non-specular diffraction intensity) but were more corrugated for the intermixed structures compared to the on-surface structures and for Na compared to K. The former was attributed primarily to the larger in-plane metallic bonding for the on-surface structures.

1. Introduction

The properties of alkali metals adsorbed on aluminum surfaces have been actively studied by many experimental and theoretical techniques [1] and therefore a great deal is known about them. The adsorption of alkalis on aluminum surfaces is somewhat different from adsorption on most other metal surfaces in that at sufficiently high temperatures, alkali metal atoms intermix with substrate atoms to form ordered surface alloys. On Al(111) this intermixing occurs at temperatures above about 200 K [2].

Helium atom interactions with alkali metal surfaces are among the weakest interactions known in nature [3]. This weakness is mainly due to the large size of the alkali atoms, which prevents He atoms from sampling the deepest part of the He–alkali van der Waals potential. One implication for the scattering of He atoms from alkali metal surfaces is that the He atoms will turn around at a distance significantly farther from the adatom nuclei than is typical for transition metal substrates. At these larger turn-around distances, the corrugation of the He–surface potential is typically smaller, leading to smaller non-specular He-diffraction intensities. This effect has been shown to be the primary cause for the very small non-specular He diffraction intensities from alkali metal overlayers on graphite [4].

The nature of alkali metal adsorption on metallic surfaces has been the subject of numerous studies and debates [5]. Low-energy He atoms as a surface probe offer information about the surface charge density in a region which is not easily accessible by most experimental techniques or by theory. He-atom scattering has been used to study various properties of alkali metal atoms adsorbed on Cu and Ni surfaces [6–15]. The intermixing of alkali metals on Al(111) offers an opportunity to study a wider range of adsorption structures than is

0953-8984/99/305735+22$30.00

usually available in any given adsorption system. For instance, potassium forms two different $(\sqrt{3} \times \sqrt{3})R30^\circ$ structures on Al(111): one in which the potassium atoms adsorb on top of Al atoms, and one in which the K atoms substitute for Al atoms [16]. The substitutional site $(\sqrt{3} \times \sqrt{3})R30^\circ$ structure can also be formed with Na atoms instead of K atoms, allowing the effect of adatom size on the surface charge density to be investigated. He-atom scattering is also sensitive to the considerable restructuring of the Al surface upon alkali metal adsorption. In this paper we summarize previous studies of Na and K adsorption on Al(111) and present new results for specular He reflection and He diffraction from Na and K on Al(111).

2. Summary of previous studies

The adsorption structures formed by Na adsorption on Al(111) have been previously studied by various techniques [1, 2] and are summarized in figure 1. At temperatures below about 200 K the Na atoms remain on top of the substrate and at a coverage of about 0.15 condense into an incommensurate structure denoted in the literature as '3×3' which gives a split-spot low-energy electron diffraction (LEED) pattern [2]. (Coverage is defined as the ratio of number of adsorbed atoms to atoms in the top layer of the unreconstructed substrate surface.) The exact locations of the adatoms are not known for this structure, but surface-core-level-shift (SCLS) spectroscopy suggests that all Na atoms are in similar sites which would imply that there are anti-phase domains, consistent with the split-spot LEED pattern. At higher coverages, above 0.4, a higher-order-commensurate (HOC) (4×4) structure forms, having nine atoms per unit cell. This structure saturates at a coverage of 0.56. A surface-extended-x-ray-absorption-fine-structure (SEXAFS) study of this structure concluded that three different sites are occupied by the adatoms and that their perpendicular spacing relative to the top Al layer varies by about 0.4 Å, depending on the site [17]. Such a large variation in height of the Na atoms above the surface might be expected to lead to a sizable corrugation of the charge density at the surface of the Na atoms.

For adsorption at temperatures above 200 K, the overlayer first condenses into a $(\sqrt{3} \times \sqrt{3})R30^\circ$ phase at a coverage of about 0.15. This structure consists of Na atoms substitutionally adsorbed (figure 1), and the proposed mechanism for the formation of this structure involves the kicking out of Al atoms from the surface, the occupation of the resulting vacancies by Na atoms, and the diffusion of the 'free' Al atoms to step edges [18]. This naturally involves a large movement of Al atoms at the surface. STM studies of the adsorption of Na onto Al(111) at 300 K support this large mass transport by the observation of a complete restructuring of the surface steps upon formation of the $(\sqrt{3} \times \sqrt{3})R30^\circ$ phase [19]. This phase saturates at a coverage of 0.33, at which point a new phase begins to develop, the (2×2) phase. The (2×2) structure has been determined by various structural techniques to consist of a surface bilayer alloy [1], in which half of the Na atoms are located beneath the first Al layer. The top layer of atoms in this case is a $p(2 \times 2)$ arrangement of Na atoms, located in fcc sites of the reconstructed substrate. The optimum coverage for this structure is 0.5, although it can be observed at higher Na coverages.

In the STM study [19], Na atoms could only be imaged when they were in the substitutional (vacancy) sites, and not when they were adsorbed on top of the surface. This was attributed to the high mobility of the non-substituted adatoms. In contrast to the earlier SCLS measurements, these STM measurements indicated that some of the Na atoms begin to substitute at very low coverages, and not just upon formation of the condensed $(\sqrt{3} \times \sqrt{3})R30^\circ$ structure. When the $(\sqrt{3} \times \sqrt{3})R30^\circ$ structure was complete, a gross change was observed in the step structure of the surface—the primary step direction changed from being parallel to the $[\bar{1}10]$ direction (as on the clean surface) to being primarily parallel to the $[\bar{1}2\bar{1}]$ direction.

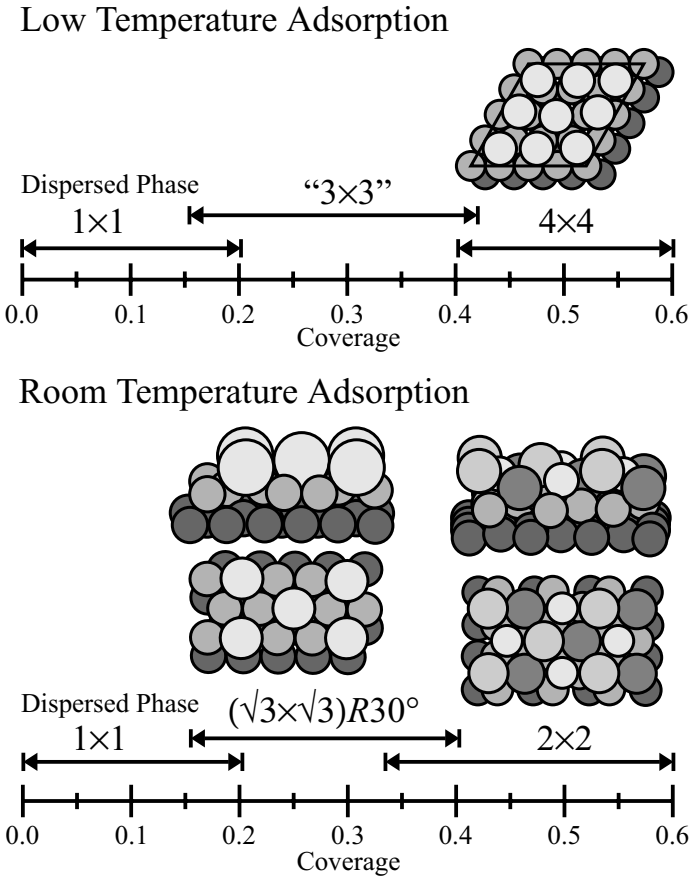

Figure 1. Schematic diagram showing the coverage dependence of the structures formed by Na adsorption on Al(111) at 100 K and 300 K [2].

The adsorption structures observed for K adsorption on Al(111) are summarized in figure 2 [2]. As for Na adsorption, 100 K adsorption resulted in structures where the K atoms occupy sites on top of the surface whereas at 300 K, intermixed structures were formed. For adsorption at 100 K, a condensed $(\sqrt{3} \times \sqrt{3})$R30° structure first begins to form at a coverage of about 0.1. This structure consists of K atoms located in the top sites. This structure saturates at a coverage of 0.33, and at higher coverages the overlayer compresses continuously until the monolayer saturates at a coverage of 0.48. Adsorption of K at 300 K looks superficially similar to the extent that a condensed $(\sqrt{3} \times \sqrt{3})$R30° phase begins to form at a coverage of 0.1. However, the geometry of this structure is quite different because the K atoms are in substitutional sites rather than top sites. The monolayer saturates when this phase is complete at a coverage of 0.33.

3. Experiment

The He-atom scattering experimental apparatus for these experiments has been described before [20]. A nearly monochromatic ($\Delta v/v = 1\%$) low-energy He beam is produced by

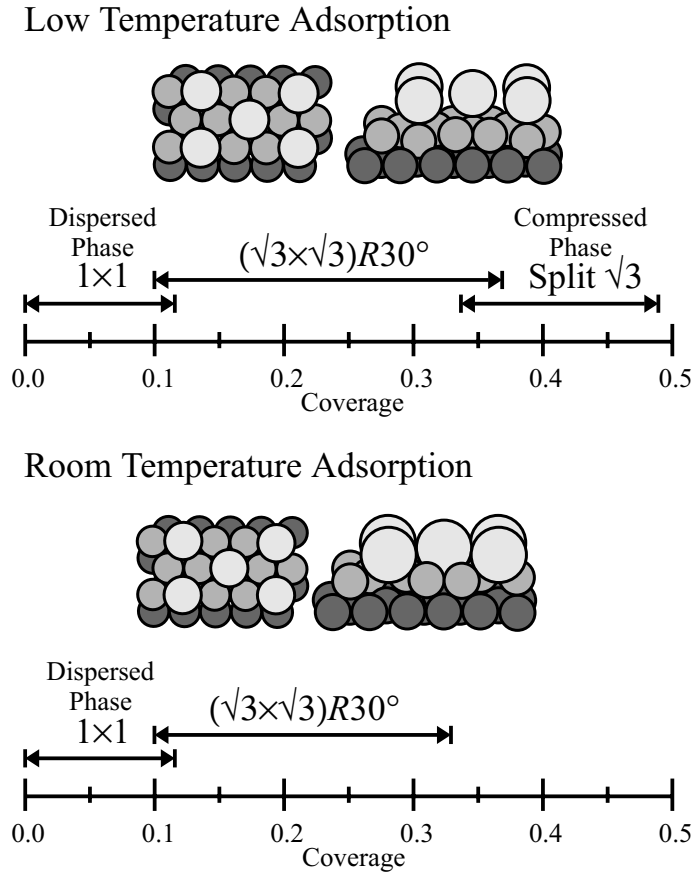

Figure 2. Schematic diagram showing the coverage dependence of the structures formed by K adsorption on Al(111) at 100 K and 300 K [2].

expanding high-pressure (20 bar) thermal He gas through a 7.5 μm nozzle cooled by liquid nitrogen. The angular divergence of the beam is about 0.1° and the diameter of the beam at the position of the sample is about 1.4 mm. The scattered He atoms are detected by a magnetic mass spectrometer in the in-plane scattering geometry with a total scattering angle fixed at 90°. The base pressure (measured using an ion gauge) of the scattering chamber is 1×10^{-10} mbar and the pressure when the He beam is on is 4×10^{-10} mbar. Low-energy electron diffraction measurements were made using a commercial rear-view LEED optics in the scattering chamber. The identification of all ordered structures was made with LEED. Auger measurements were made using a single-pass CMA analyser.

The Al(111) crystal was prepared by cutting and polishing to within 0.25° of the (111) planes using 0.25 μm grit-size diamond polishing paste. In UHV the crystal was cleaned by successive cycles of 1.5 keV Ar^+ ion bombardment and annealing to as high as 500 °C. From tests using different sputtering conditions, it is clear that the high energy of the Ar^+ ions leads to increased faceting compared to 0.5 keV Ar^+ ions. We used the higher energy because the scattering from facets facilitated the observation of the surface restructuring. The test of the

cleanliness of the surface was the reproducibility of an intense specularly scattered He beam, which was more sensitive than Auger electron spectroscopy to impurities. The alkali-metal atoms were evaporated onto the Al surface from a shielded, collimated SAES Getters alkali metal source which was located 8 cm from the Al surface such that adsorption could be carried out simultaneously with the measurement of scattered He intensities. The size of the alkali beam at the sample was the same as the sample size. Accurate dosing was facilitated by a shutter in front of the alkali source shield aperture. The pressure during dosing was less than 4×10^{-11} mbar.

4. Results

4.1. Adsorption curves

This section presents data for measurements of the He specular intensity as a function of alkali coverage. The scans were performed at a constant dosing rate, which was typically one-half monolayer per minute, in the $[\bar{1}10]$ scattering azimuth. The alkali coverage scale was determined by observation of the LEED patterns at various points of the curve and comparison of these to earlier studies [2]. The dose scale is actually a time scale, but for convenience is calibrated to represent coverage, i.e. the ratio of overlayer atoms to top-layer substrate atoms. This was done by comparison to the LEED patterns. The actual coverages above a saturated layer may be different due to changes in sticking coefficient, but this appears to be true only for 300 K adsorption. Each measurement was done at two different beam energies, 16.7 meV and 23 meV, respectively, which correspond to in-phase and anti-phase scattering with respect to two terraces separated by a single-layer Al(111) step, the height of which is 2.34 Å. The corresponding perpendicular momentum transfers are 8.00 Å^{-1} for the in-phase condition and 9.40 Å^{-1} for the anti-phase condition.

Figure 3 shows the specular He intensity at the two beam energies as a function of Na coverage while the Al(111) crystal was held at 100 K. The main features of these curves are a rapid decrease of intensity starting with the beginning of adsorption, a subsequent increase which becomes a maximum at the completion of the (4×4) structure (coverage $= 0.56$) and several subsequent minima and maxima which correspond to the layer-by-layer growth of Na. These oscillations are rapidly damped, but extend out to at least four layers.

At a very low dose (~ 0.06 coverage) there is a slight increase in slope of the curve which we attribute to a changeover from adsorption primarily at defect sites (steps) to adsorption primarily on terraces. The coverage at which the change in slope occurs implies that about 10% of the first-layer Na atoms adsorb first at defect sites. (The exact location of this 'kink' feature varied from run to run and generally moved somewhat higher during the course of these experiments—we attribute this to varying degrees of roughening of the surface due to the cleaning treatment and alkali adsorption.) The location of the first minimum is at a coverage of about 0.15, which is the coverage where a LEED pattern of the condensed '3×3' phase is first observed [2]. There is a slight change in slope of the adsorption curves at a coverage of 0.45, which corresponds to the onset of formation of the commensurate (4×4) structure [2]. This structure is completed at a coverage of 0.56, which corresponds to the first maximum of specular intensity. Assuming a constant sticking coefficient, subsequent maxima occur at coverages of 1.05, 1.55 and 2.0. The highest intensity of scattering from the overlayer is not as high as the original intensity from the substrate for in-phase scattering. The damping of the intensity of subsequent layers of Na is consistent with a decreasing effective Debye temperature for subsequent layers, as deduced previously for alkali metal films on Cu and Ni surfaces [11, 12].

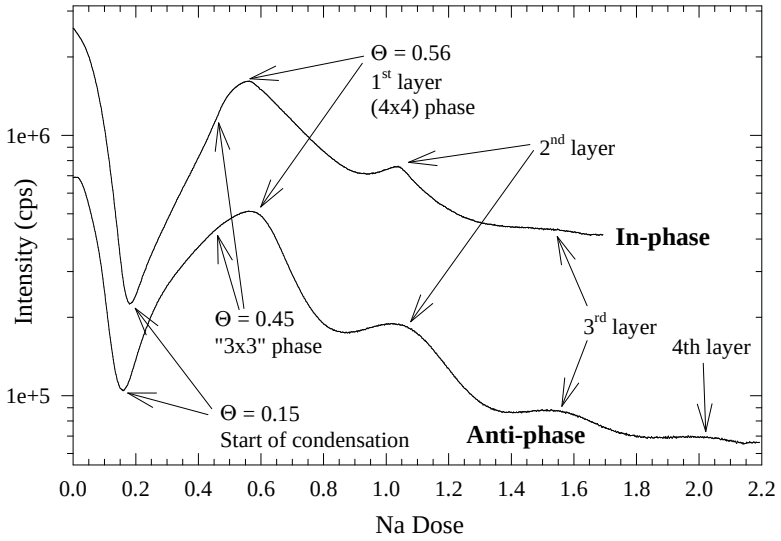

Figure 3. Specular He-beam intensity (in counts per second) during dosing Na on Al(111) at 100 K. The two curves were taken at in-phase (Δk-perpendicular $= 8.0$ Å^{-1}) and anti-phase (Δk-perpendicular $= 9.4$ Å^{-1}) conditions with respect to Al–Al steps. The Na dose scale was calibrated by observation of the LEED pattern. The dose scale corresponds to coverage, i.e. it represents the ratio of the number of overlayer atoms per top-layer substrate atoms. The main adsorption features are labelled on the curves (see text).

Figure 4 shows the sodium adsorption curves at 300 K. Here, the kink due to crossover from defect adsorption to terrace adsorption occurs at a somewhat higher coverage, 0.1, indicating that a larger number of Na atoms are initially adsorbed at defects. This could be due to the higher mobility of the Na atoms at 300 K, but the restructuring of the Al surface upon Na adsorption may also contribute to this effect, as discussed later. The first minimum in the curves occurs at a coverage of 0.15, which is the onset of condensation as observed in earlier studies [2], and the first maximum occurs at a coverage of 0.33, where the $(\sqrt{3} \times \sqrt{3})$R30° monolayer is complete. A second peak is observed in the 'in-phase' curve (seen as a kink in the 'anti-phase' curve) which corresponds to the formation of the (2×2) surface alloy. At higher coverages, the specular intensity continues to decrease, indicating that there are additional structure changes which occur at higher Na doses, but there is no evidence for layer-by-layer growth of Na as there was at 100 K.

Figures 5 and 6 show the adsorption curves for potassium. At 100 K, potassium also appears to grow in a layer-by-layer mode, although the subsequent peaks are more damped than for the case of Na, presumably due to the lower Debye temperature of potassium (100 K) compared to Na (150 K) [21]. The kink due to defect adsorption occurs at a coverage of about 0.08 and the first minimum occurs at a coverage of 0.15, which is near the onset of condensation as observed in previous studies [2]. The first maximum occurs at a coverage of 0.45 which corresponds to a compressed incommensurate layer of K, determined by observation of the LEED pattern. A commensurate $(\sqrt{3} \times \sqrt{3})$R30° structure was observed in the LEED pattern at a coverage of 0.33, but no special feature was observed in the adsorption curves. There is a reproducible kink in the anti-phase adsorption curve at a coverage of 0.4, however, which we cannot explain. Subsequent maxima corresponding to second- and third-layer

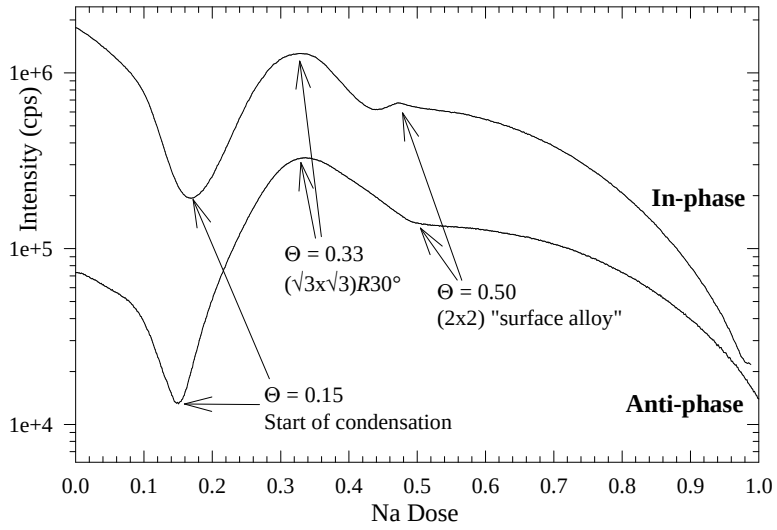

Figure 4. Specular He-beam intensity during dosing Na on Al(111) at 300 K. The two curves were taken at the in-phase and anti-phase conditions with respect to Al–Al steps. The Na dose scale was calibrated by observation of the LEED pattern. The dose scale was calibrated to correspond to coverage, i.e. it represents the ratio of the number of overlayer atoms per top-layer substrate atom. The main adsorption features are labelled on the curves (see text).

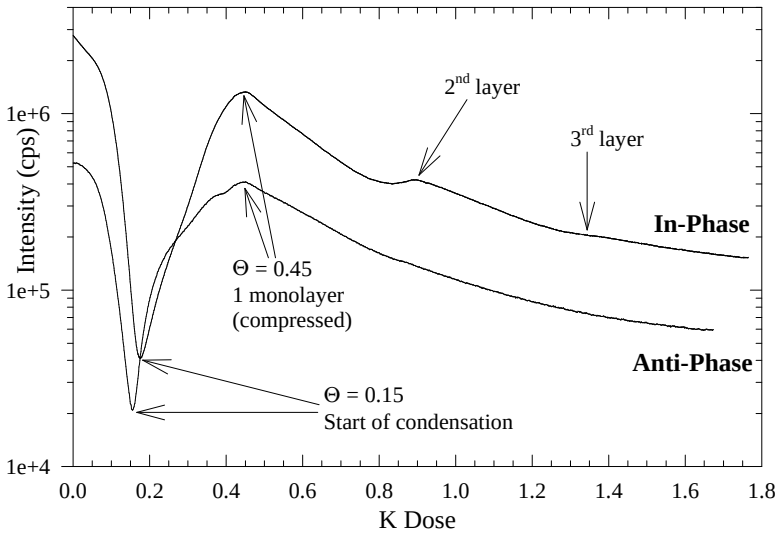

Figure 5. Specular He-beam intensity during dosing K on Al(111) at 100 K. The two curves were taken at the in-phase and anti-phase conditions with respect to Al–Al steps. The K dose scale was calibrated by observation of the LEED pattern. The dose scale corresponds to coverage, i.e. it represents the ratio of the number of overlayer atoms per top-layer substrate atoms. The main adsorption features are labelled on the curves (see text).

completion are observed at coverages of 0.89 and 1.37, respectively (assuming a constant sticking coefficient).

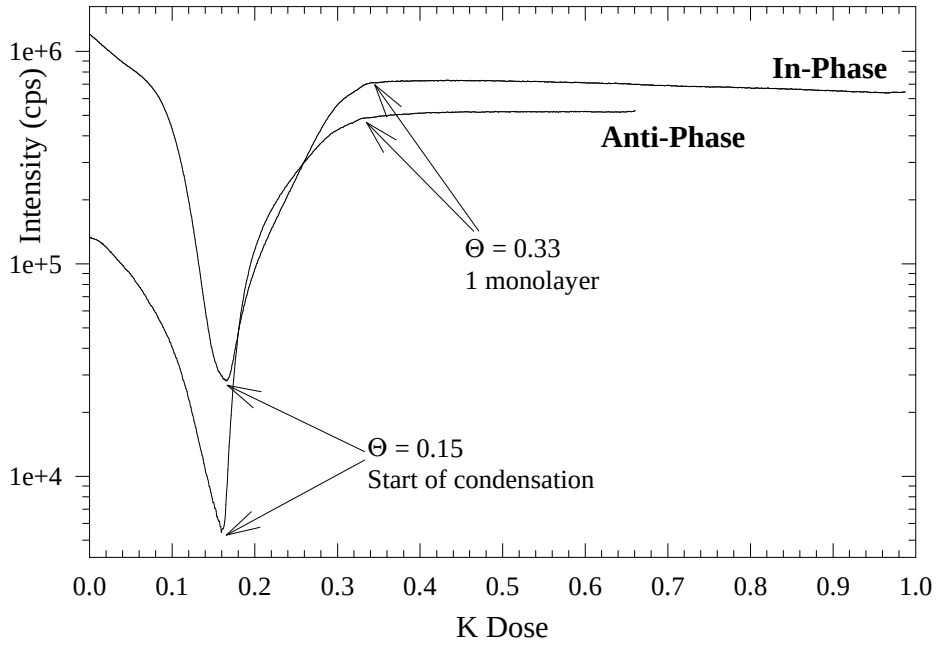

Figure 6. Specular He-beam intensity during dosing K on Al(111) at 300 K. The two curves were taken at the in-phase and anti-phase conditions with respect to Al–Al steps. The K dose scale was calibrated by observation of the LEED pattern. The dose scale corresponds to coverage, i.e. it represents the ratio of the number of overlayer atoms per top-layer substrate atoms. The main adsorption features are labelled on the curves (see text).

Table 1. Summary of features observed in adsorption curves. Typical errors in coverage determination are ±0.04. Calculations for the diffuse cross-sections were based on the adsorption curves from the in-phase scattering condition.

Feature	Na, 100 K	Na, 300 K	K, 100 K	K, 300 K
Location of defect 'kink'	0.06	0.1	0.08	0.1
Location of first minimum	0.15	0.15	0.15	0.15
Monolayer completion	0.56	0.33	0.45	0.33
Second layer completion	1.05	—	0.89	—
Third layer completion	1.55	—	1.37	—
Fourth layer completion	2.00	—	—	—
Diffuse elastic scattering cross-section (Å^2)	53	55	66	69

At 300 K, potassium does not grow in a layer-by-layer mode. Rather, its coverage saturates at a coverage of 0.33 (consistent with room-temperature adsorption of K on other metal surfaces [1]), which corresponds to the $(\sqrt{3} \times \sqrt{3})R30^\circ$ structure. The kink due to defect adsorption occurs at a coverage of about 0.1, the same as found for Na at 300 K, and the minimum occurs at a coverage of about 0.15, somewhat higher than the onset of condensation as observed in an earlier study [2]. The adsorption curve rises until a coverage of 0.33 is reached, and then stays constant, implying that no further K adsorbs on the surface at 300 K. The features of all of the adsorption curves are summarized in table 1.

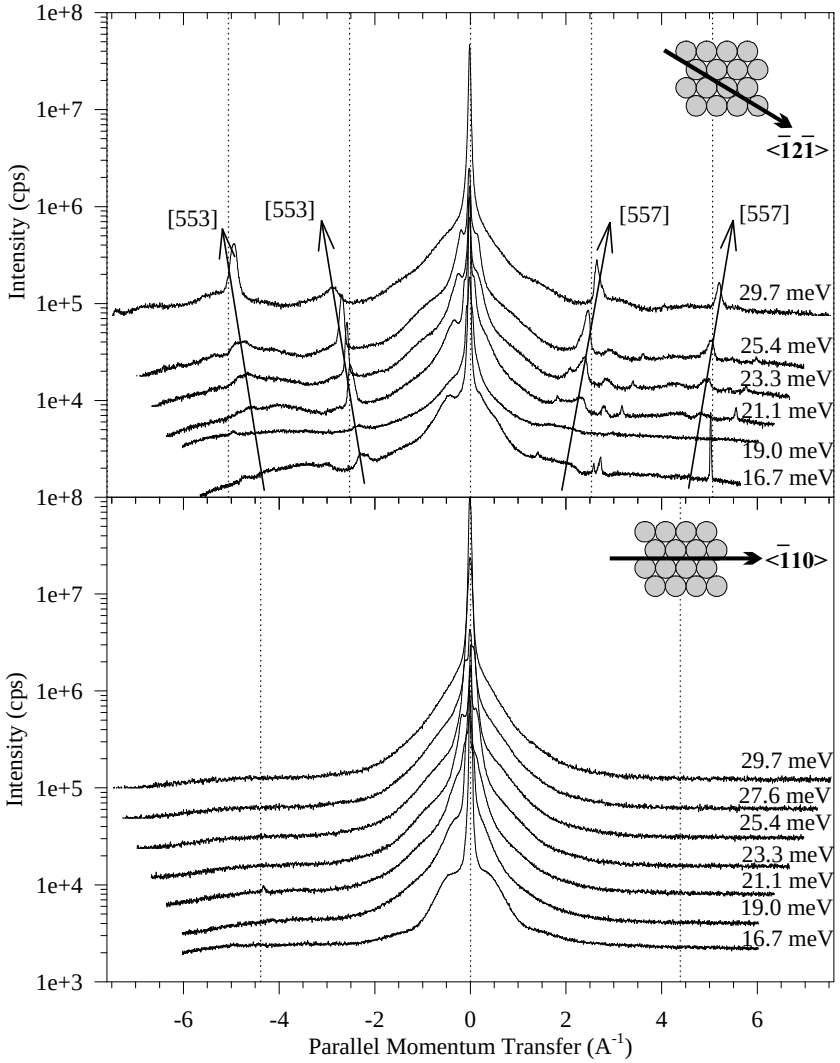

Figure 7. Angular scans taken for clean Al(111) along the [$\bar{1}2\bar{1}$] and [$\bar{1}10$] scattering azimuths (shown schematically in the insets), as a function of parallel momentum transfer. The curves at different beam energies (indicated on curves) are offset for clarity. The directions corresponding to the primary facet peaks observed are indicated. Vertical lines show the anticipated locations of diffraction beams.

4.2. Angular scans

Figure 7 shows angular scans taken for the clean Al(111) substrate at 300 K along the [$\bar{1}2\bar{1}$] and [$\bar{1}10$] azimuths. The scans are labelled with the incident beam energies, and the insets indicate the scattering directions of the scans. The largest feature in each of these scans is the specular reflection. There are also shoulders on the specular peaks, and a considerable number of off-specular peaks are present in the [$\bar{1}2\bar{1}$] azimuth. These peaks are clearly not diffraction

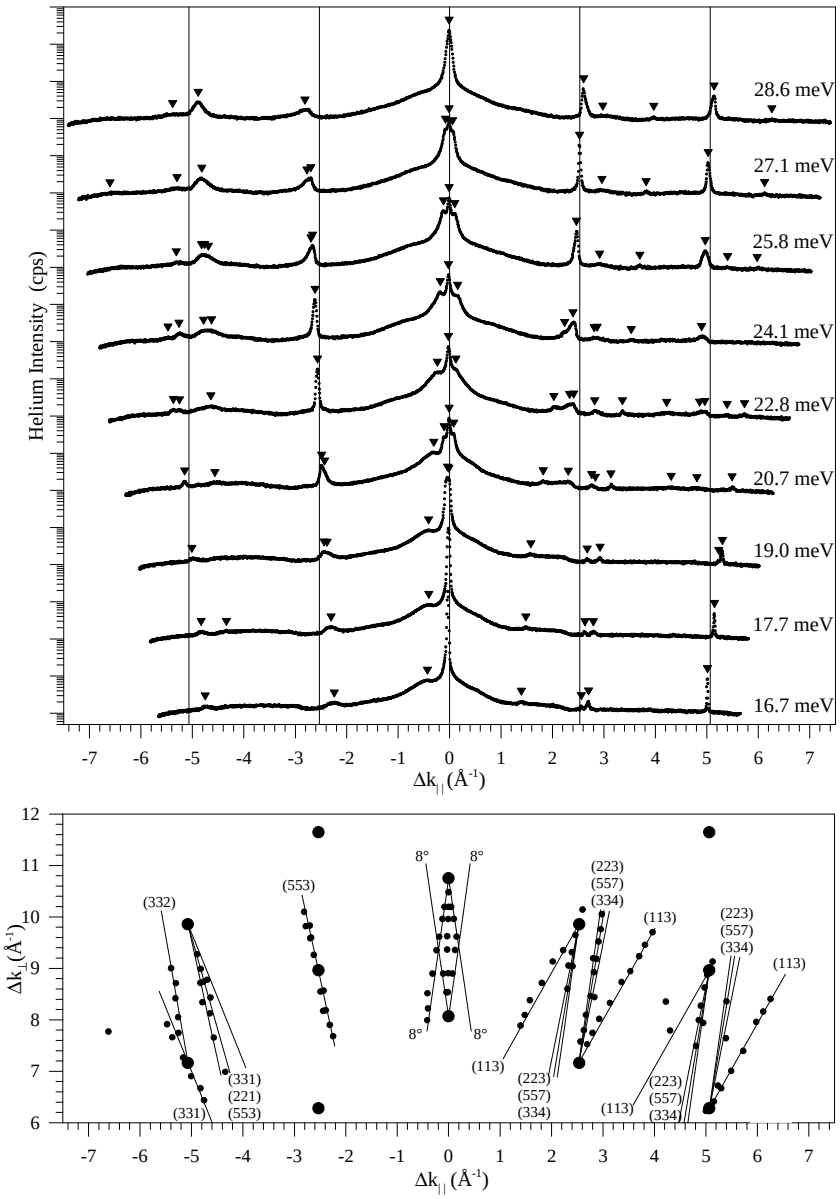

Figure 8. Angular scans for clean Al(111) along the $[\bar{1}2\bar{1}]$ azimuth. The positions of all peaks in these scans are indicated. The locations of these peaks in k-space are plotted in the lower graph. The facets are identified by the slope of the lines traced by these peaks in k-space. A diffraction peak from the (111) facets would be indicated as a vertical line on such a k-space diagram.

peaks from the (111) surface since they disperse with increasing beam energy. To determine the nature of these peaks, they were identified and their positions plotted in k-space, as shown in figure 8 for the $[\bar{1}2\bar{1}]$ azimuth. It is readily seen that these peaks have a linear dispersion

in k-space, which is consistent with scattering from facets. Also noted on the k-space graph are the positions of the 3D Bragg points. It can be observed that the intensities of the peaks become a maximum when they coincide with a 3D Bragg peak. The variation of intensity is due to the destructive interference which takes place between wavefronts scattering from successive planes. The in-phase conditions coincide with the 3D Bragg points. This effect is also seen in the specular peak. The identification of the primary facets is made by measuring the angles (relative to vertical) of the lines traced out by the peaks in k-space and identifying which facets are inclined at that angle relative to the (111) plane. All peaks which scatter from a given facet will disperse at the same angle in k-space. The facets thus identified are indicated on the figure. While there are many facets in the $[\bar{1}2\bar{1}]$ azimuth, the only evidence for facets in the $[\bar{1}10]$ azimuth are the shoulders on the specular beam itself.

Facets can be thought of as areas having highly correlated steps. The scans in figure 7 indicate that there is a significant density of steps on the clean Al(111) surface at 300 K, and that the majority of the steps run largely parallel to the $[\bar{1}10]$ azimuth. (Note that steps running parallel to $[\bar{1}10]$ will show up most strongly in the $[\bar{1}2\bar{1}]$ scattering azimuth.) This is consistent with an STM study which concluded that the preferred step orientations on the clean surface are mostly along the $[\bar{1}10]$ azimuth, and never along the $[\bar{1}2\bar{1}]$ azimuth [19]. (In fact, there are apparently some steps along this direction as the shoulders on the specular peak in the $[\bar{1}10]$ are due to facets having long-period ($\sim$ 17 atomic rows) terraces [22].) The peaks due to facets become sharper as the crystal is annealed, up to 530 K.

A comparison of the integrated intensities under the facet peaks relative to the (111) specular peak suggests that 3–5% of the surface is composed of facets having terrace widths of less than about 10 Å. The sharpness of the facet peaks (and the (111) specular peak) at the 3D Bragg conditions indicate that the underlying crystal has a very small mosaic spread, less than 0.2°. The width of the (111) specular peak at other scattering conditions indicates at the average terrace width is at least 140 Å [22, 23], and since many steps are correlated (forming facets) this suggests that away from the facets, some terraces may be considerably wider. Non-specular diffraction peaks could not be detected from the clean surface. First-order diffraction peaks in the $[\bar{1}2\bar{1}]$ azimuth were observed in a previous He-diffraction study of Al(111) [24] at an intensity 10^{-4} times lower than the specular intensity. This is on the limit of detectability in the present study, and these peaks, if present, are obscured by the scattering from facets.

Figure 9 shows angular scans for the substitutional $(\sqrt{3} \times \sqrt{3})R30^\circ$ structure of Na at 300 K. The most striking aspect of these scans, when compared to those from the clean surface, is that almost all of the scattering from facets has disappeared in the $[\bar{1}2\bar{1}]$ azimuth, while there are now separate non-specular peaks in the $[\bar{1}10]$ azimuth. The absence of facet scattering in the $[\bar{1}2\bar{1}]$ azimuth has two possible interpretations—either the facets have been covered incoherently by Na atoms or they have disappeared from the surface. The coverage dependence of the angular scans, shown in figure 10, indicates that both effects contribute to the observation. The facet peaks in the $[\bar{1}2\bar{1}]$ scattering azimuth have largely disappeared by a coverage of 0.10, indicating that the defect-site Na atoms obscure the Al facets. The facet peaks in the $[\bar{1}10]$ scattering azimuth, however, begin to show up at a coverage of 0.15 and continue to grow as the coverage increases. Thus, the formation of facets which correspond to steps parallel to the $[\bar{1}2\bar{1}]$ direction coincides with the formation of the substitutional $(\sqrt{3} \times \sqrt{3})R30^\circ$ structure. This is consistent with the earlier STM study which found that the preferred direction for steps on the $(\sqrt{3} \times \sqrt{3})R30^\circ$-covered surface was parallel to the $[\bar{1}2\bar{1}]$ direction, i.e. the close-packed direction of the $(\sqrt{3} \times \sqrt{3})R30^\circ$ structure [19], and therefore would be observed in the $[\bar{1}10]$ scattering azimuth. The fact that these facet peaks are evident at all when the surface is covered by Na indicates that Na atoms on these facets are commensurate with the facet structure. In addition to the peaks from facets, there are also non-dispersing peaks in the $[\bar{1}10]$ scan which

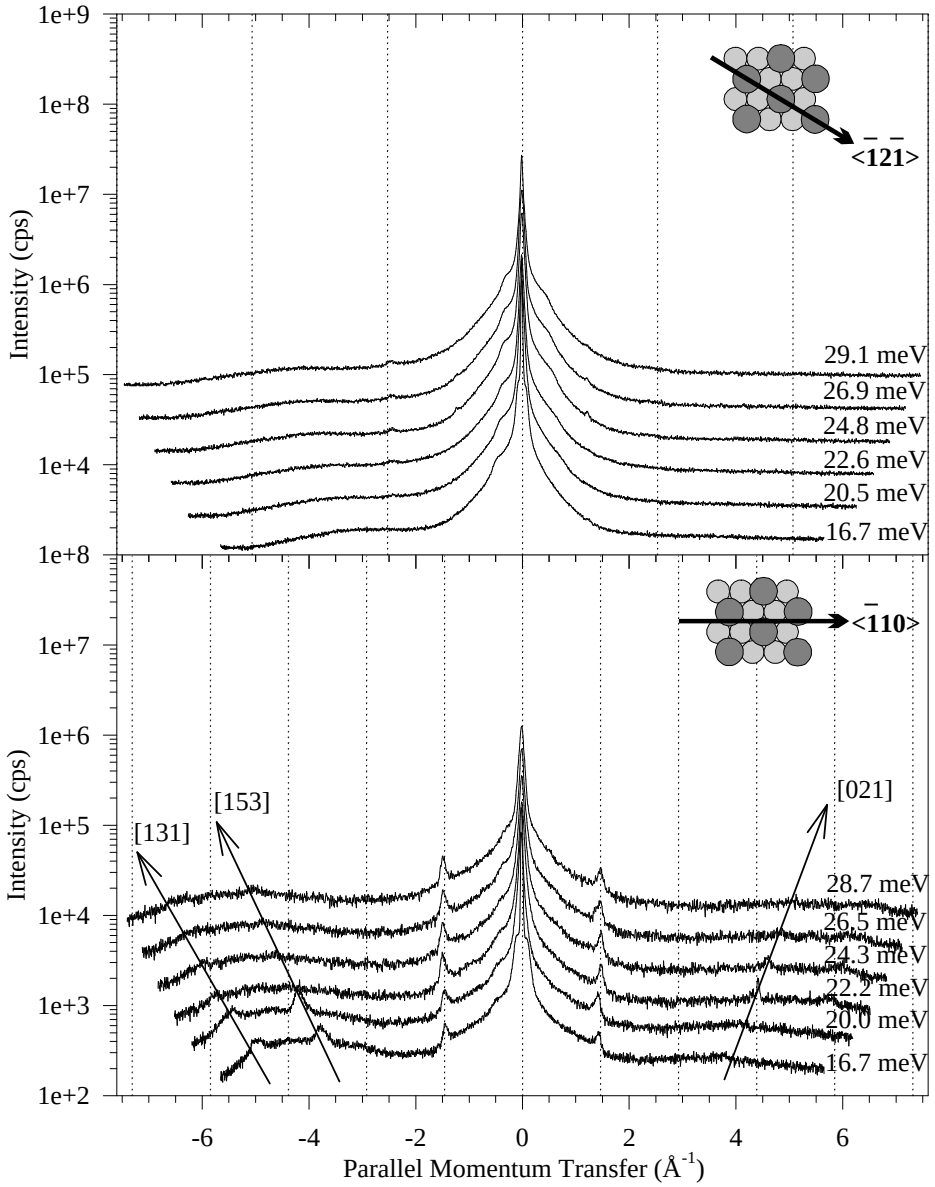

Figure 9. Angular scans for the 300 K structure Al(111)–($\sqrt{3} \times \sqrt{3}$)R30°–Na along the [$\bar{1}2\bar{1}$] and [$\bar{1}10$] scattering azimuths for different incident beam energies. The insets show these azimuths relative to the ($\sqrt{3} \times \sqrt{3}$)R30° structure. The curves at different beam energies (indicated on curves) are offset for clarity. Vertical lines show the anticipated locations of diffraction beams from the ($\sqrt{3} \times \sqrt{3}$)R30° structure.

correspond to diffraction from the ($\sqrt{3} \times \sqrt{3}$)R30°–Na overlayer. The location of these peaks is consistent with the first-order diffraction peaks expected for a ($\sqrt{3} \times \sqrt{3}$)R30° overlayer, and their intensities are given in table 2.

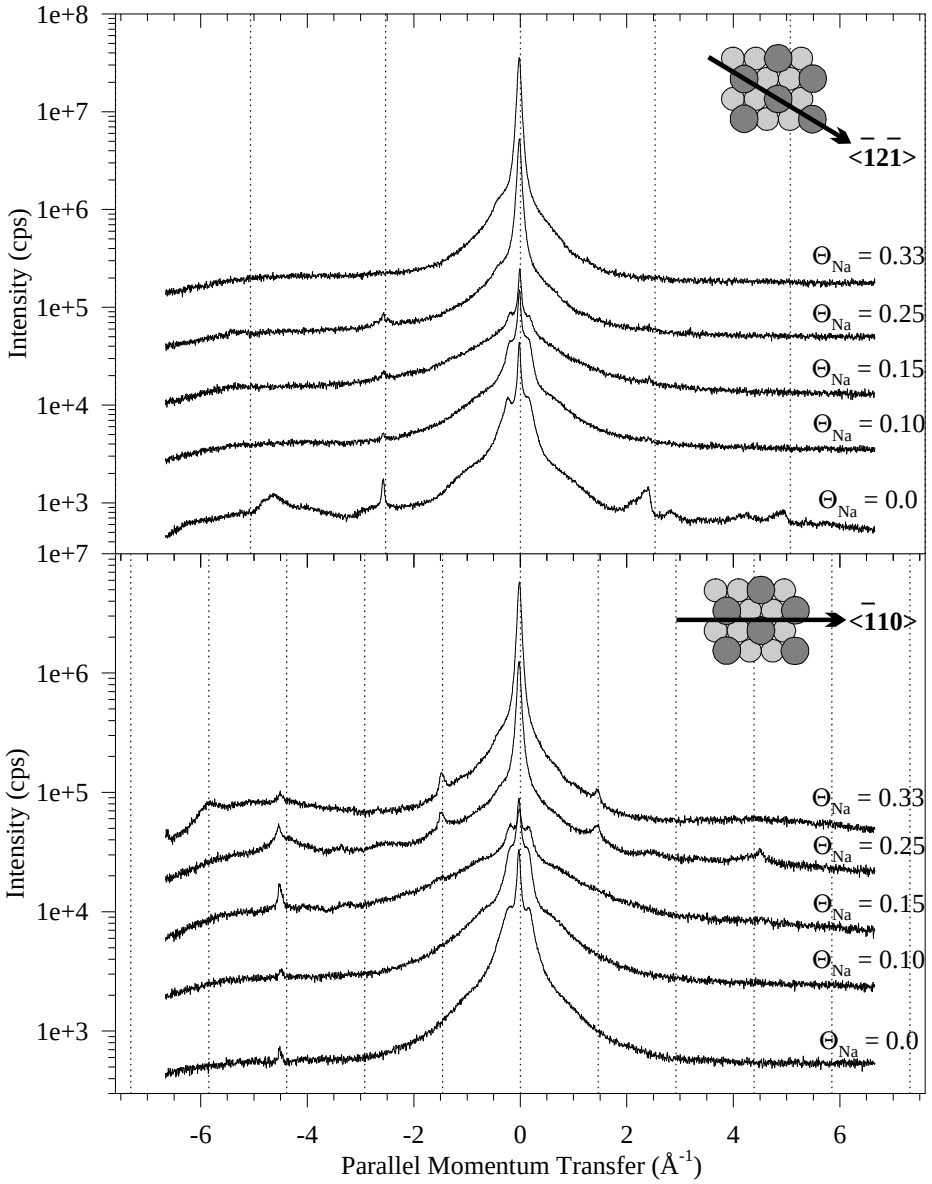

Figure 10. Angular scans as a function of coverage for the substitutional Al(111)–($\sqrt{3}\times\sqrt{3}$)R30°–Na along the [$\bar{1}2\bar{1}$] and [$\bar{1}10$] scattering azimuths at a beam energy of 23.2 meV. It can be readily seen that most of the facet scattering has disappeared from the [$\bar{1}2\bar{1}$] azimuth already at 0.10 coverage. Facet scattering in the [$\bar{1}10$] scattering azimuth is already evident at a coverage of 0.15. Vertical lines indicate locations of diffraction beams from the ($\sqrt{3}\times\sqrt{3}$)R30° structure.

Figure 11 shows angular scans from the surface alloy (2 × 2) phase of Na/Al(111) at 300 K and 0.5 coverage. At this coverage there is little evidence left of the facets in either azimuth, and the diffraction peaks can be easily seen along both azimuths. The

Table 2. He-atom diffraction integrated intensities observed for alkali metal overlayers relative to the specular intensity. Detectability limits in these experiments are generally around $I/I_0 = 5 \times 10^{-4}$. HOC denotes a higher-order commensurate phase. The measured intensities for equivalent beams (e.g. (10) and (−10)) were averaged. SAO refers to a charge density calculated from a superposition of atomic orbitals, whereas DFT refers to charge density calculated in density functional theory [30]. The similarity of the intensities calculated for the two K structures is due to the fact that the Al charge density is very small at the location of the He-atom interaction with the surface. The calculations were for an incident beam energy of 16.8 meV.

	$I(10)/I(00)$	$I(20)/I(00)$	$I(21)/I(00)$
Al(111)–($\sqrt{3} \times \sqrt{3}$)R30°–Na, substitutional site			
Experiment	1.2×10^{-2}	$<10^{-5}$	1×10^{-4}
Calculated (SAO)	1.3×10^{-2}	2.5×10^{-5}	3.0×10^{-4}
Calculated (DFT)	1.7×10^{-4}	5.0×10^{-9}	5.0×10^{-8}
Al(111)–(2 × 2)–2Na, intermixed structure			
Experiment	0.30	9.4×10^{-3}	4.0×10^{-2}
Calculated (SAO)	5×10^{-2}	5×10^{-4}	4×10^{-3}
Al(111)–($\sqrt{3} \times \sqrt{3}$)R30°–K, substitutional site			
Experiment	$<10^{-4}$	$<10^{-4}$	6×10^{-4}
Calculated (SAO)	2.1×10^{-3}	7.6×10^{-7}	9.7×10^{-6}
Al(111)–($\sqrt{3} \times \sqrt{3}$)R30°–K, top site			
Experiment	$<10^{-4}$	$<10^{-4}$	$<10^{-4}$
Calculated (SAO)	2.1×10^{-3}	7.6×10^{-7}	9.7×10^{-6}

larger diffraction intensities indicate that the more-open (2 × 2) structure produces a more highly corrugated potential for He scattering. Some slight facet intensity in the $[\bar{1}2\bar{1}]$ azimuth suggests that the step direction may have again changed to being mostly parallel to the $[\bar{1}10]$ direction, which would be consistent to being parallel to the close-packed rows of the (2 × 2) structure.

For the 100 K adsorption of Na where no restructuring of the surface was previously observed, the substrate facet peaks disappear upon sodium adsorption, indicating again that the Na atoms adsorbed on the facets are not commensurate with the facet structure. No diffraction features were observed for dosing at this temperature except for the HOC (4 × 4) structure. Figure 12 shows scans in the $[\bar{1}2\bar{1}]$ azimuth for this structure at a sample temperature of 100 K. Small diffraction peaks can be observed at parallel momentum transfers of ± 1.90 Å^{-1} which correspond to the third-order diffraction peaks of the (4 × 4) structure. If the Na adatoms were uniformly spaced at identical heights, then only the third-order peaks (which correspond to the first-order peaks for a lattice which has a period which is 4/3 the Al–Al distance) would be visible. There are also some barely visible first-order peaks at momentum transfers of ± 0.63 Å^{-1}, suggesting that there is some lattice relaxation in the overlayer structure, resulting in an overall 4 × 4 period instead of a $4/3 \times 4/3$ period.

Potassium forms the same substitutional ($\sqrt{3} \times \sqrt{3}$)R30° structure as Na at 300 K [2]. Figure 13 shows angular scans for this structure. As for Na adsorption, the facets in the $[\bar{1}2\bar{1}]$ azimuth have disappeared and pronounced facet scattering can be seen in the $[\bar{1}10]$ azimuth. Therefore it appears that the same type of restructuring which occurs for 300 K Na adsorption also occurs for K adsorption. Weak diffraction intensity from the overlayer in the $[\bar{1}2\bar{1}]$ azimuth is observed, whereas none is observed in the $[\bar{1}10]$ azimuth, which is the direction of the strongest diffraction intensity for the same structure of Na. Any diffraction intensity in this azimuth is obscured by the strong facet scattering, which results in intensity *dips* and other fine structure features in the angular scans. Energy-resolved measurements indicate that these dips are part of the elastic scattering, and their origin is most likely the same

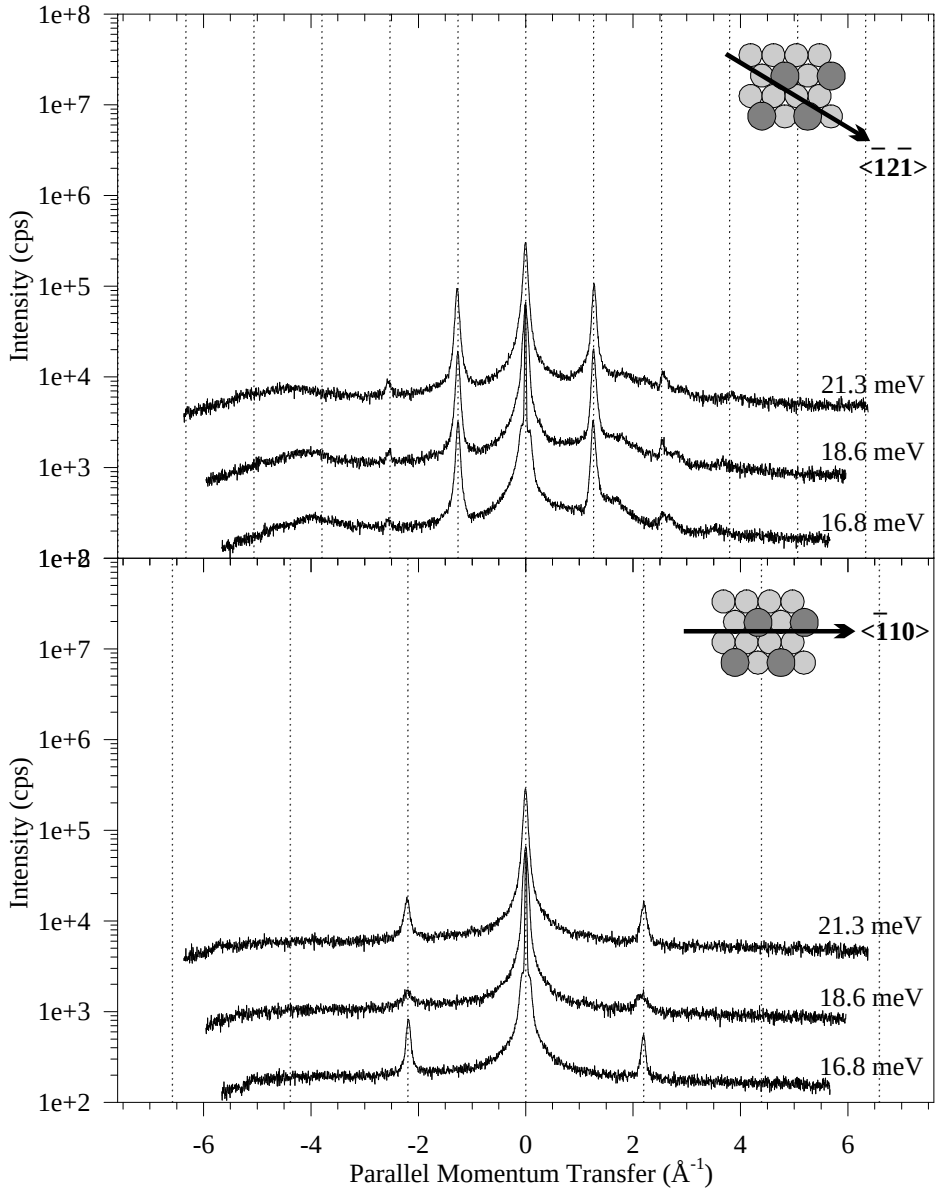

Figure 11. Angular scans for the 300 K structure Al(111)–(2 × 2)–Na along the [$\bar{1}2\bar{1}$] and [$\bar{1}10$] scattering azimuths. The insets show these azimuths relative to the (2 × 2) structure. The curves at different beam energies (indicated on curves) are offset for clarity. Vertical lines show the anticipated locations of diffraction beams from the (2 × 2) structure.

as the facet-related peaks in other scans. Similar features have been seen in elastic scattering studies and simulations of close-packed surfaces with large densities of correlated step edges (i.e. facets; see figure 6 in [25]).

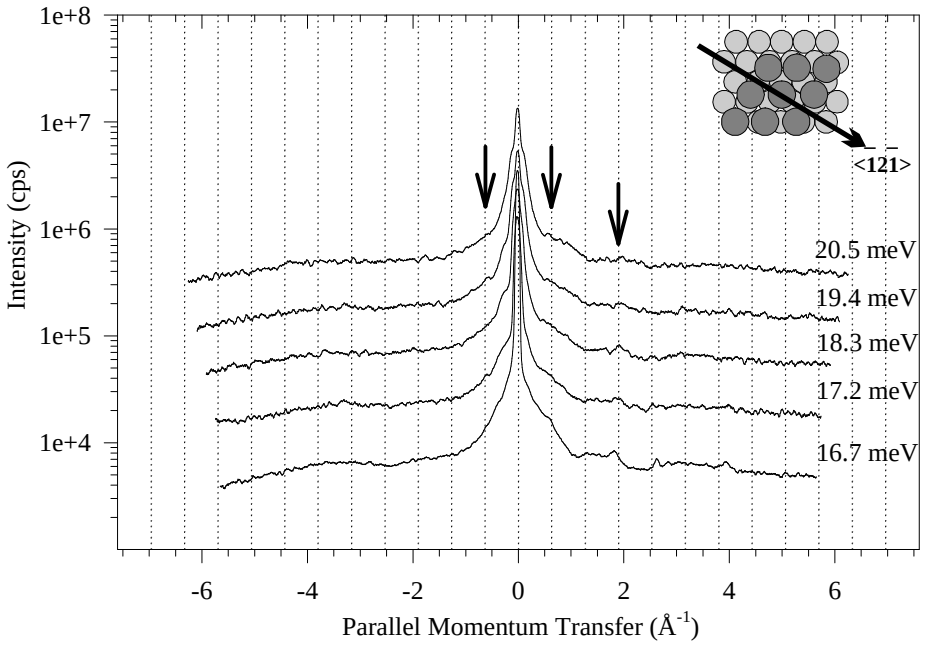

Figure 12. Angular scans for the 100 K structure Al(111)–(4 × 4)–Na along the [$\bar{1}2\bar{1}$] scattering azimuth. The curves at different beam energies (indicated on curves) are offset for clarity. Vertical lines show the anticipated locations of diffraction beams from the (4 × 4) structure. The noise level is different on these scans because they were taken more rapidly in order to minimize contamination which has a larger effect at low coverages.

Figure 14 shows angular scans at 100 K for the top-site ($\sqrt{3} \times \sqrt{3}$)R30° structure of potassium. As for the case of Na adsorption, the facet peaks which are present on the clean surface in the [$\bar{1}2\bar{1}$] azimuth have largely disappeared, most likely due to diffuse scattering from incommensurate K atoms on the facets. In this case, we note that there are no new facet peaks observed in the [$\bar{1}10$] azimuth since restructuring apparently does not occur. Nor is there any discernible diffraction intensity from the overlayer ($\sqrt{3} \times \sqrt{3}$)R30° structure.

5. Discussion

The general shape of all of the adsorption curves indicates that the first atoms adsorbed on the surface migrate to surface defects, primarily to extended defects such as surface steps. When these sites are saturated, which appears to occur at coverages of 0.06 to 0.10, the next atoms apparently adsorb on terraces, and, as these adatoms are more isolated, they each have a larger effective scattering cross-section. There appears to be more defect-related (step) adsorption at 300 K than at 100 K. Since the mobility of alkali adatoms is very high at low coverages on flat surfaces, even at 100 K [10], we attribute this difference to a higher occupation of alkali adatoms on defect sites at 300 K. This indicates a difference in the adsorption geometry at steps for the two temperatures, suggesting that intermixing occurs at the steps at low coverages for 300 K adsorption, although intermixing does not occur on the terraces until after condensation occurs [2]. This is consistent with the STM study which observed some intermixed Na even at low coverages [20].

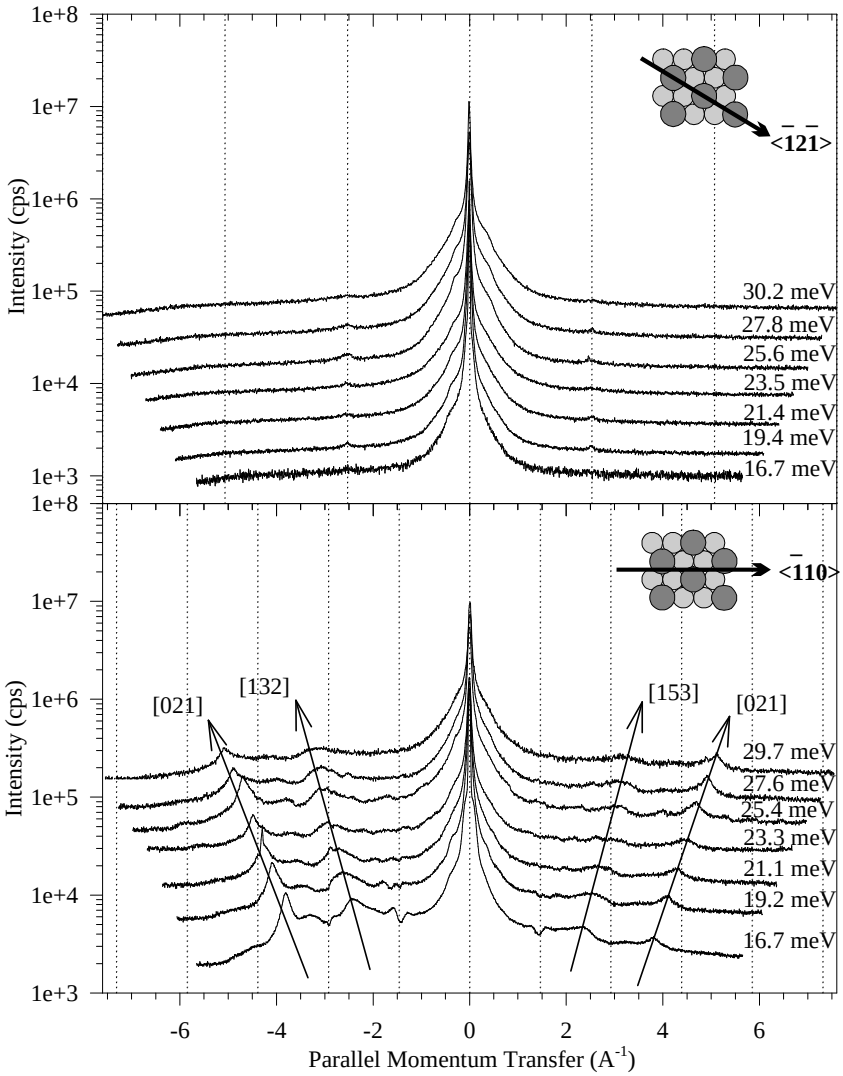

Figure 13. Angular scans for the 300 K structure Al(111)–($\sqrt{3} \times \sqrt{3}$)R30°–K along the [$\bar{1}2\bar{1}$] and [$\bar{1}10$] scattering azimuths. The insets show these azimuths relative to the ($\sqrt{3} \times \sqrt{3}$)R30° structure. The curves at different beam energies (indicated on curves) are offset for clarity. Vertical lines show the anticipated locations of diffraction beams from the ($\sqrt{3} \times \sqrt{3}$)R30° structure. The directions corresponding to the primary facet peaks observed are indicated.

The presence of isolated defects such as single adsorbed atoms (at low densities) results in diffuse elastic scattering which causes a reduction of the specular reflectivity, given by

$$I/I_0 = 1 - n\sigma$$

where n is the number of adsorbed atoms per unit area, σ is the cross-section for diffuse-elastic scattering from these atoms and I_0 is the intensity at zero coverage [26]. Therefore the slope of the adsorption curve in the regime where adatoms are adsorbing on terraces can be

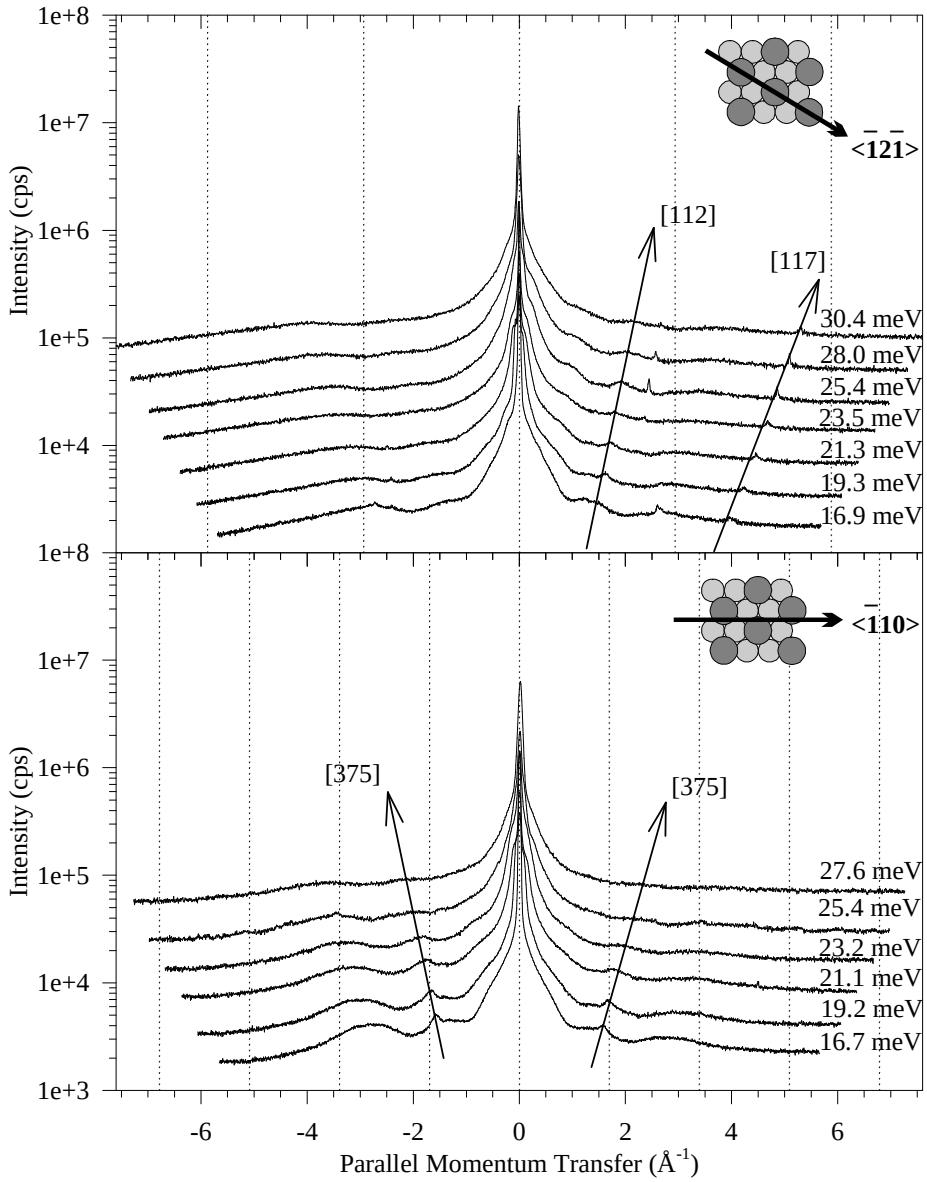

Figure 14. Angular scans for the 100 K structure Al(111)–($\sqrt{3} \times \sqrt{3}$)R30°–K along the [$\bar{1}2\bar{1}$] and [$\bar{1}10$] scattering azimuths. The insets show these azimuths relative to the ($\sqrt{3} \times \sqrt{3}$)R30° structure. The curves at different beam energies (indicated on curves) are offset for clarity. Vertical lines show the anticipated locations of diffraction beams from the ($\sqrt{3} \times \sqrt{3}$)R30° structure.

used to calculate the cross-section for diffuse scattering for the adatom. The results of these calculations are shown in table 1. The cross-section is larger for K than for Na, as might be expected since the atomic radius of K is about 25% larger than that of Na. However, there is little if any difference between the cross-sections for the 100 K versus 300 K adsorption.

Since one might expect different cross-sections for on-surface adsorption and substitutional-site adsorption, this result is consistent with the earlier SCLS results which indicated that the adatoms do not intermix on *terraces* until the $(\sqrt{3} \times \sqrt{3})R30^\circ$ structure begins to form [2]. These cross-section numbers are significantly smaller, however, than the values of 100–130 $Å^2$ found in other studies for alkali adsorption on metal surfaces [9, 11]. This difference may be due to the relatively large number of defects already present on this clean Al(111) surface which will effectively reduce the diffuse scattering cross-section of the adatoms.

For Na adsorption at 100 K, the coverages for the multilayers are slightly lower than the expected multiple of the monolayer coverage, and therefore the average density of the subsequent layers is lower than that of the monolayer. Since the monolayer density is similar to that observed in bulk Na [1], the lower dose required for subsequent layers suggests that there are vacancies in the subsequent layers of Na, perhaps due to slow equilibration at the low adsorption temperature. The coverages of the subsequent peaks in the K adsorption curve at 100 K are close to the expected multiples of the monolayer coverage, suggesting that the kinetics governing growth are faster for K than for Na at 100 K. The general decrease in the amplitude of the oscillations observed for multilayer adsorption is consistent with both an increase in surface defects and a decrease in the overlayer Debye temperature with increasing film thickness, as found for K and Rb overlayers on Ni(100) [11, 12]. We note that the Debye temperatures of the bulk alkalis (100 K for K, 150 K for Na) are significantly lower than that of bulk Al (428 K).

For 300 K adsorption, there is no layer-by-layer growth of the alkali films. For potassium, the coverage saturates at the $(\sqrt{3} \times \sqrt{3})R30^\circ$ phase and there is no subsequent change in the specular intensity upon dosing. For sodium, a subsequent peak appears upon formation of the (2×2) surface alloy at a coverage of 0.5, and at higher dosing the specular intensity continues to decrease, implying that there is some further adsorption of Na. Other studies have suggested that Na continues to intermix above a coverage of 0.5 [2]. When the dosing was stopped at nominal coverages of 0.33 or 0.50, the specular intensity increased somewhat for several minutes, implying that the kinetics of restructuring at the higher coverages is somewhat slower than the dosing. This is consistent with the STM study which indicated that diffusion of a Na–vacancy pair is considerably slower than that of single Na atoms on the surface [19].

The angular scans taken from the clean Al(111) surface are consistent with earlier STM measurements which indicated that surface steps run primarily parallel to the $[\bar{1}10]$ direction [27]. Results for adsorption of Na or K at 300 K are also consistent with the STM measurements [27] which indicated that the primary step direction changes upon formation of the $(\sqrt{3} \times \sqrt{3})R30^\circ$ structure to being parallel to the $[\bar{1}2\bar{1}]$ direction, i.e. parallel to the close-packed Na rows. In contrast to the STM study, however, the angular scans indicate that the steps in the $[\bar{1}2\bar{1}]$ direction begin to form in the same coverage range where the $\sqrt{3}$ structure begins to form, and not only at the completion of the $\sqrt{3}$ structure. For adsorption at both 100 K and 300 K, we attribute the disappearance of the facet peaks in the $[\bar{1}2\bar{1}]$ scattering azimuth (steps parallel to the $[\bar{1}10]$ direction) to disordered adsorption at the step edges. However, since more adatoms appear to be involved in the step-site adsorption at 300 K, we believe that intermixing occurs at steps even before the formation of the ordered structure on the terraces. This is consistent with the STM study which suggests that intermixing does occur at steps before overlayer condensation [20]. Facets in the $[\bar{1}10]$ scattering azimuth were visible even after adsorption of the alkali overlayer, indicating that the alkali adsorbed coherently on those facets. We note that the steps are considerably rougher in this direction, as shown in figure 15, which shows a (112) surface (with steps parallel to the $[\bar{1}10]$ direction) and a (132) surface (with steps parallel to the $[\bar{1}2\bar{1}]$ direction). Therefore a structure in which the adatoms are coherent with the substrate is more likely for the facets in this direction, consistent with the observation.

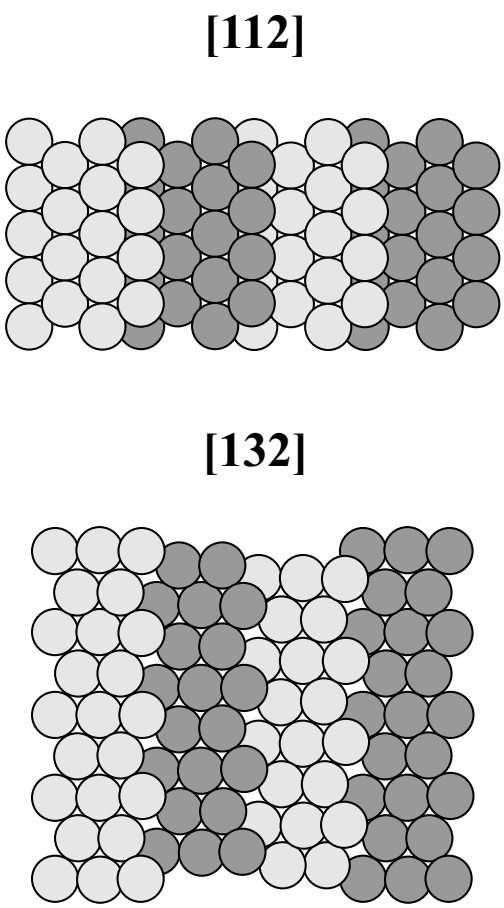

Figure 15. Schematic drawings showing the geometry of single-atom steps in the $[\bar{1}2\bar{1}]$ and the $[\bar{1}10]$ azimuths. The actual planes shown are the (211) plane and the (231) plane.

Table 2 lists the relative diffraction intensities observed for the alkali overlayers along with relative intensities which have been calculated using atomic charge densities and a numerical coupled-channels calculation [22, 28]. Generally, the trends in the observed intensities are those expected on the basis of the lateral spacing of the top-layer atoms relative to the atom 'sizes' (i.e. their natural bulk spacing). For instance, the largest diffraction intensities are observed for the (2×2) Na surface alloy phase, shown in figure 1, in which the top-layer Na atoms are spaced 5.72 Å apart, which is quite separated compared to the metallic Na–Na distance of 3.82 Å. For the identical $(\sqrt{3} \times \sqrt{3})R30^\circ$ substitutional structures (adatom NN spacing $=$ 4.96 Å) of Na (metallic NN spacing $=$ 3.82 Å) and K (metallic NN spacing $=$ 4.72 Å), the non-specular diffraction intensity is larger for Na than for K. These results all indicate a larger He–surface corrugation when the adatom spacing is large compared to its size. We also note that the diffraction intensities are generally larger for the intermixed structures than the on-surface structures, which is consistent with the smoother surface which might be expected from a more 'metallic' intralayer bonding observed in density-functional-

theory (DFT) calculations of these surfaces [29, 30]. This is also consistent with the extremely small diffraction intensities observed for the monolayer phase of Na of Cu(100) where the diffraction to specular ratio was about 10^{-5} [15], and the lack of observation of diffraction intensities from alkalis on graphite [4].

For comparison, diffraction intensities were calculated using a numerical coupled-channels calculation which used the surface charge densities as input. These charge densities were approximated by a superposition of atomic charge densities, a technique which was shown to somewhat overestimate the potential corrugation in an earlier study of alkalis on graphite [4, 31]. The diffraction intensity calculations here neglected both the attractive part of the He–surface potential and thermal effects, both of which would be expected to decrease the intensity. Nevertheless, the calculated intensities were somewhat smaller than those observed for the intermixed Na structures. Using a charge density from a DFT calculation for the $(\sqrt{3} \times \sqrt{3})$R30° structure [32], even smaller diffraction intensities were obtained.

Anomalously large diffraction intensities might occur if there were significant coherent scattering from the facets into these locations of k-space, which would be expected to occur when the scattering conditions are near to a 3D Bragg point. However, the intensities of these diffraction peaks did not vary appreciably with beam energy, indicating that this diffraction intensity is from the flat terraces. The observation of large diffraction intensities could conceivably occur if there is a large degree of charge transfer toward the substrate from the outermost Na atoms. There is significant charge redistribution toward the substrate in adsorbed alkali metals, although the effect of this on the corrugation at the location of the He-atom turn-around distance has not been quantified [29, 33, 34].

The small diffraction intensities observed for the on-surface HOC (4×4) phase of Na are also larger than would be expected from a flat close-packed Na overlayer (not calculated) but may be consistent with a structure in which the adatoms have height variations of more than 0.4 Å as found in the SEXAFS measurements [17]. Clearly some variation within the HOC unit cell must be present since first-order diffraction peaks are observed, and a uniform overlayer would give peaks only at the 3/4 positions.

6. Conclusion

We have presented He-atom scattering results from adsorption studies for Na and K on Al(111). Features in the adsorption curves at coverages of one monolayer and lower were identified with ordered structures observed with LEED and which have been previously studied by other techniques. The adsorption cross-sections of isolated alkali adatoms on the terraces were calculated to be in the range 50–70 Å^2.

Adsorption at 100 K proceeds in a layer-by-layer growth mode for up to at least four Na layers and three K layers, whereas K adsorption saturates at one layer at 300 K. An additional slow restructuring of the surface apparently occurs upon further adsorption of Na at 300 K.

The scattering from correlated surface steps (facets) provided strong evidence for significant mass transport during the formation of the intermixed structures [19]. The primary step direction was observed to change from parallel to $[\bar{1}10]$ on the clean surface to parallel to $[\bar{1}2\bar{1}]$ on the intermixed surface. This means that the primary step direction changes from being parallel to the close-packed direction on clean Al(111) to being parallel to the close-packed direction on Al(111)–$(\sqrt{3} \times \sqrt{3})$R30°–alkali. There is some evidence (small facet peaks) which indicates that the primary step direction may change back upon formation of the (2×2) structure.

Non-specular diffraction intensities were significantly higher for 300 K adsorption than for 100 K adsorption, suggesting that the intermixed surfaces are more corrugated than the on-

surface structures. This is consistent with the increased intralayer metallic bonding observed in DFT calculations of these overlayers [29, 33, 34]. The diffraction intensities calculated assuming a superposition of atomic charge densities were generally smaller than those observed in the experiments. This suggests that there may be a significant rearrangement (depletion) of the charge density at the location of the He-atom interaction with the surface.

Acknowledgments

We gratefully acknowledge J F Annett for providing the program for calculating He-diffraction intensities and for many useful discussions. We thank C Stampfl for providing us with DFT charge densities and other useful information about the DFT calculations. We are very grateful to J Spizuoco for the data acquisition software development. We also thank J Hinch and E Conrad for useful discussions about He-atom diffraction from facets. This work has been supported by NSF grants DMR-9022681 and DMR-9629715.

References

[1] Diehl R D and McGrath R 1996 *Surf. Sci. Rep.* **23** 43
[2] Andersen J N, Lundgren E, Nyholm R and Qvarford M 1993 *Surf. Sci.* **289** 307
[3] Cole M W, Cheng E, Carraro C, Saam W F, Swift M R and Treiner J 1994 *Physica* B **197** 254
[4] Cui J, White J D, Diehl R D, Annett J F and Cole M W 1992 *Surf. Sci.* **279** 149
[5] Diehl R D and McGrath R 1997 *J. Phys.: Condens. Matter* **9** 951
[6] Benedek G, Ellis J, Reichmuth A, Ruggerone P, Schief H and Toennies J P 1992 *Phys. Rev. Lett.* **69** 2951
[7] Ellis J and Toennies J P 1993 *Phys. Rev. Lett.* **70** 2118
[8] Ellis J and Toennies J P 1994 *Surf. Sci.* **317** 99
[9] Reichmuth A, Graham A P, Bullman H G, Allison W and Rhead G E 1994 *Surf. Sci.* **307–309** 34
[10] Senet P, Toennies J P and Witte G 1998 *Chem. Phys. Lett.* **299** 389
[11] Flach B, Hulpke E and Steinhögl W 1998 *Surf. Sci.* **412/413** 12
[12] Hulpke E, Lower J and Reichmuth A 1996 *Phys. Rev.* B **53** 13 901
[13] Graham A P, Hofmann F, Toennies J P, Chen L Y and Ying S C 1997 *Phys. Rev. Lett.* **78** 3900
[14] Graham A P, Hofmann F, Toennies J P, Chen L Y and Ying S C 1997 *Phys. Rev.* B **56** 10 567
[15] Graham A P and Toennies J P 1997 *Phys. Rev.* B **56** 15 378
[16] Stampfl C, Scheffler M, Over H, Burchhardt J, Nielsen M M, Adams D L and Moritz W 1994 *Phys. Rev.* B **49** 4959
[17] Schmalz A, Aminpirooz S, Haase J, Batchelor D R, Nielsen M M , Bøgh E and Adams D L 1994 *Surf. Sci.* **301** L211
[18] Neugebauer J and Scheffler M 1992 *Phys. Rev.* B **46** 16 067
[19] Brune H, Wintterlin J, Behm R J and Ertl G 1995 *Phys. Rev.* B **51** 13 592
[20] Cui J, Jung D R and Frankl D R 1990 *Phys. Rev.* B **42** 9701
[21] Ashcroft N W and Mermin N S 1976 *Solid State Physics* (Philadelphia, PA: Holt, Rinehart and Winston)
[22] Lakin J 1998 *PhD Thesis* Penn State University
[23] Lu T-M and Lagally M G 1980 *Surf. Sci.* **99** 695
[24] Hinch B J, Doak R B and Dubois L H 1993 *Surf. Sci.* **286** 261
[25] Hinch B J and Toennies J P 1990 *Phys. Rev.* B **42** 1209
[26] Poelsema B and Comsa G 1989 *Scattering of Thermal Energy Atoms from Disordered Surfaces* (Berlin: Springer)
[27] Barth J V, Brune H, Schuster R, Ertl G and Behm R J 1993 *Surf. Sci.* **292** L769
[28] Huston J M and Schwartz C 1983 *J. Chem. Phys.* **79** 5179
[29] Stampfl C, Neugebauer J and Scheffler M 1994 *Surf Sci.* **307–309** 8
[30] Stampfl C and Scheffler M 1995 *Surf. Rev. Lett.* **2** 317
[31] White J D, Cui J, Strauss M, Diehl R D, Ancilotto F and Toigo F 1994 *Surf. Sci.* **307–309** 1134
[32] Stampfl C 1998 private communication
[33] Stampfl C, Neugebauer J and Scheffler M 1994 *Surf. Rev. Lett.* **1** 213
[34] Stampfl C, Scheffler M, Over H, Burchhardt J, Nielsen M M, Adams D L and Moritz W 1992 *Phys. Rev. Lett.* **69** 1532